Scripta Materialia 227 (2023) 115301

Contents lists available at ScienceDirect

Scripta Materialia

journal homepage: www.journals.elsevier.com/scripta-materialia

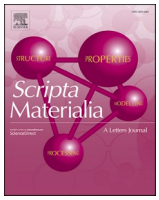

A novel approach for producing Mg-3Al-1Zn-0.2Mn alloy wire with a promising combination of strength and ductility using CoreFlow™

Xingjian Zhao [a], Xun Zeng [a,b], Liang Yuan [a,d], Joao Gandra [c], Qamar Hayat [e,f], Mingwen Bai [e], W Mark Rainforth [a], Dikai Guan [a,b,*]

[a] Department of Materials Science and Engineering, University of Sheffield, Sheffield S1 3JD, UK
[b] Department of Mechanical Engineering, University of Southampton, Southampton SO17 1BJ, UK
[c] TWI, Granta Park, Great Abington, Cambridge CB21 6AL, UK
[d] College of Bioresources Chemical and Materials Engineering, Shaanxi University of Science and Technology, Xi'An 710021, China
[e] Centre for Manufacturing and Materials, Coventry University, Coventry CV1 5FB, UK
[f] Warwick Manufacturing Group (WMG), The University of Warwick, Coventry CV4 7AL, UK

ARTICLE INFO

Keywords:
CoreFlow™
Stationary shoulder friction stir extrusion
Mg alloys
Ductility
EBSD

ABSTRACT

Mg-3Al-1Zn-0.2Mn (wt.%, AZ31B) wires were successfully produced from commercial hot-rolled plates in one step using the CoreFlow™ process, a novel stationary shoulder friction stir extrusion manufacturing. CoreFlowed AZ31B wires exhibited fine grains with a heterogeneous grain size distribution of 6.5 ± 4.2 μm along the transverse direction (TD) compared with the as-received material. A weakened texture was also obtained in CoreFlowed AZ31B, with basal poles aligned parallel to TD shift toward extrusion direction (ED) from wire center to edge. Periodic needle-like regions with a distinctively different orientation from neighbouring regions were observed at the sample edge. The engineering ultimate tensile strength (UTS) and elongation (El) of the CoreFlowed sample was 258 ± 5 MPa and 22.3 ± 0.8%. The El was significantly increased by 58% with equivalent UTS compared to the as-received material. Such a good combination of strength and ductility is attributed to grain refinement with heterogeneity, texture weakening, and homogeneously redistributed second phase particles.

Magnesium is the lightest metallic structural material (the density of Mg is 2/3 of aluminium, and only 2/9 of steel) [1]. Mg alloys have been increasingly used in products which aim at mass reduction for energy saving, carbon emission reduction, and efficiency improvement [2–4]. However, the application of Mg alloys is still far less than that of Al alloys and steel. One of the reasons for this is the limited formability of Mg alloys at room temperature [5,6]. Mg has a hexagonal close-packed (HCP) crystal structure and the deformation mode is relatively limited. Among common deformation modes, basal slip and extension twinning have much lower critical resolved shear stress (CRSS) at low temperatures compared with other deformation modes, and thus non-basal slip systems are usually not activated to facilitate continuous plastic deformation [7,8]. As a result, producing Mg alloys with high strength and ductility remains a challenge.

To solve the aforementioned problem, many strategies have been investigated. Adding rare-earth (RE) elements [9–11] or Ca [12,13] into Mg has been proved to be effective due to the possibility of texture weakening. Controlling deformation path is also an approach which can possibly solve this problem by texture weakening [14,15]. Severe plastic deformation (SPD) [16] is another possible solution which aims at solving the problem by refining the grain size. Grain refinement can increase the yield strength, and improve ductility by increasing the activity of intergranular deformation [7,17,18], supress the formation of extension twinning [18], and enhance the synergetic plastic deformation in neighbouring grains [7]. So far, many SPD variants have been applied to Mg alloys [19], including equal channel angular pressing, high pressure torsion, accumulative roll bonding, friction stir processing (FSP), etc. Although grain refinement was achieved, there are still some limitations such as limited size [20,21], several repetitive steps, and extra pre-treatments between steps [22–24]. Thus, SPD technologies with reduced steps and continuous or semi-continuous technology remain challenging.

CoreFlow™ is a new SPD and sub-surface treatment technology developed from friction stir welding (FSW), recently invented by TWI

* Corresponding author at: Department of Mechanical Engineering, University of Southampton, Southampton SO17 1BJ, UK.
E-mail address: dikai.guan@soton.ac.uk (D. Guan).

https://doi.org/10.1016/j.scriptamat.2023.115301
Received 30 November 2022; Received in revised form 4 January 2023; Accepted 8 January 2023
Available online 11 January 2023

(Fig. S1, Video S1). In this paper, CoreFlow™ was used to produce Mg alloy wires for the first time. It was designed as a subsurface channelling technology [25,26]. However, we found CoreFlow™ has a potential of rapidly screening chemical compositions for high performance metallic wires and producing bespoke wires of theoretically unlimited lengths from the base material in a single step without extra external heat input. CoreFlow™ is believed to have similar effects on Mg alloys to what FSP can possibly do, such as grain refinement, second phase particle redistribution, texture modification and thus improving the mechanical properties [27–32]. To validate our hypotheses, as-received AZ31B plates were used for wire extrusion. Various combinations of rotational speed and travel speed of the probe were tested to explore whether wire extrusion by CoreFlow™ is suitable for Mg alloys, and the tool design can be found in Fig. S1. Comparisons were made between CoreFlow™ and as-received AZ31B to reveal the texture and microstructure evolution and their effects on final mechanical properties. The findings in this work could provide insights into the potential of producing suitable Mg alloy wires for industrial applications in one step at room temperature.

As-received hot rolled AZ31B plates were used for the CoreFlow™ experiments. Based on TWI's previous experience on processing Mg and Al alloys using FSP, the traverse speed of the tool was fixed at 100 mm/min and the rotational speed was set from 600 to 1400 rpm, with an interval of 200 rpm. Texture and grain size of the wire and as-received material were characterised using a JEOL JSM-7900F FEG-SEM with EBSD detector (step size: 0.5 um for CoreFlowed samples, 2 um for as-received samples), and analyzed using AZtec Crystal software. A FEI Inspect F50 FEG-SEM was used for obtaining back-scattered electron (BSE) images to analyze the second phase particle distribution. To better understand the second phase particles in extruded wire, X-ray computed tomography (XCT) was carried out using Zeiss Xradia 620 Versa (voxel size: 2.2 um). Tensile tests were carried out on a Deben CT500 rig (details in Fig. S2, loading rate: 1.0 mm/min). Tensile tests were conducted along the RD for the as-received samples and along the ED for the CoreFlowed samples. Three tensile tests for each material were conducted.

The trial of 1200 rpm tool rotational speed was the only setting which produced consolidated wire (Fig. S3). The EBSD inverse pole figure (IPF) maps of CoreFlowed and as-received AZ31B are shown in Figs. 1 and S4. Their corresponding pole figures (PFs) and IPFs are shown in Fig. 2. The as-received AZ31B sample exhibited equiaxed grains. The average grain size of as-received AZ31B was measured to be 20.5 ± 9.4 μm, 20.7 ± 9.2 μm, and 20.0 ± 9.1 μm along RD, TD, and ND, respectively. The pole of (0001) basal planes aligned along ND with multiples of uniform density (MUD) of 9.5, indicating a strong basal texture. The average grain size of CoreFlowed AZ31B was 6.5 ± 4.2 μm and 6.7 ± 4.5 μm along TD and ED, respectively. The PFs of CoreFlowed AZ31B show that basal poles orientation was quite uncommon, and the highest texture intensity is only about 7.8 MUD (Fig. 3(a-2)). For the EBSD IPF map of CoreFlowed sample, it is evident that grains from the center to the edge are dominantly characterised by different crystal orientations with distinct geometries, which was not observed in the as-received samples. And at the edge region, periodically distributed needle-like regions dominated by grains with different colours from neighbouring regions were observed.

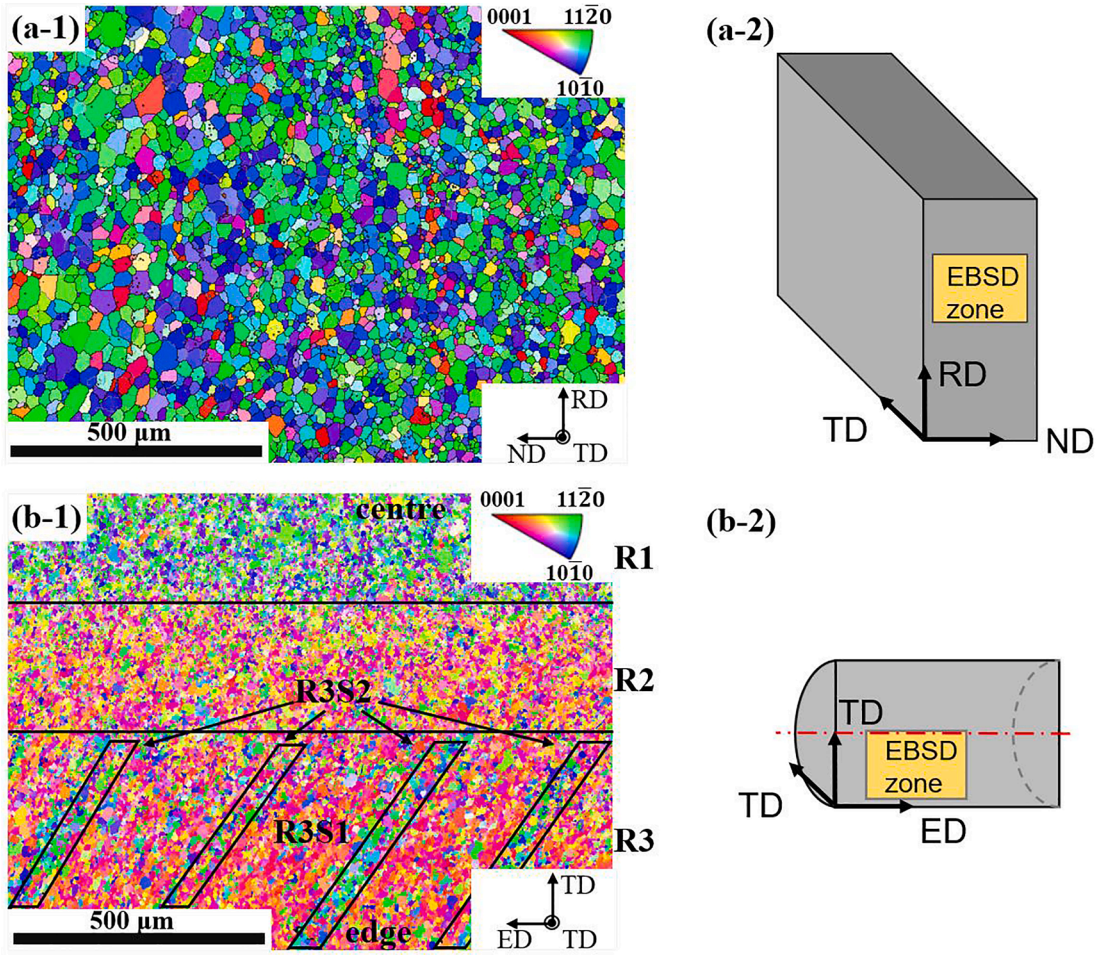

Fig. 1. (a-1) EBSD IPF map of as-received AZ31B along TD (IPF-Z//TD), (a-2) position of EBSD zone on as-received sample; (b-1) EBSD IPF map of CoreFlowed AZ31B along TD (IPF-Z//ED), (b-2) position of EBSD zone on CoreFlowed zone.

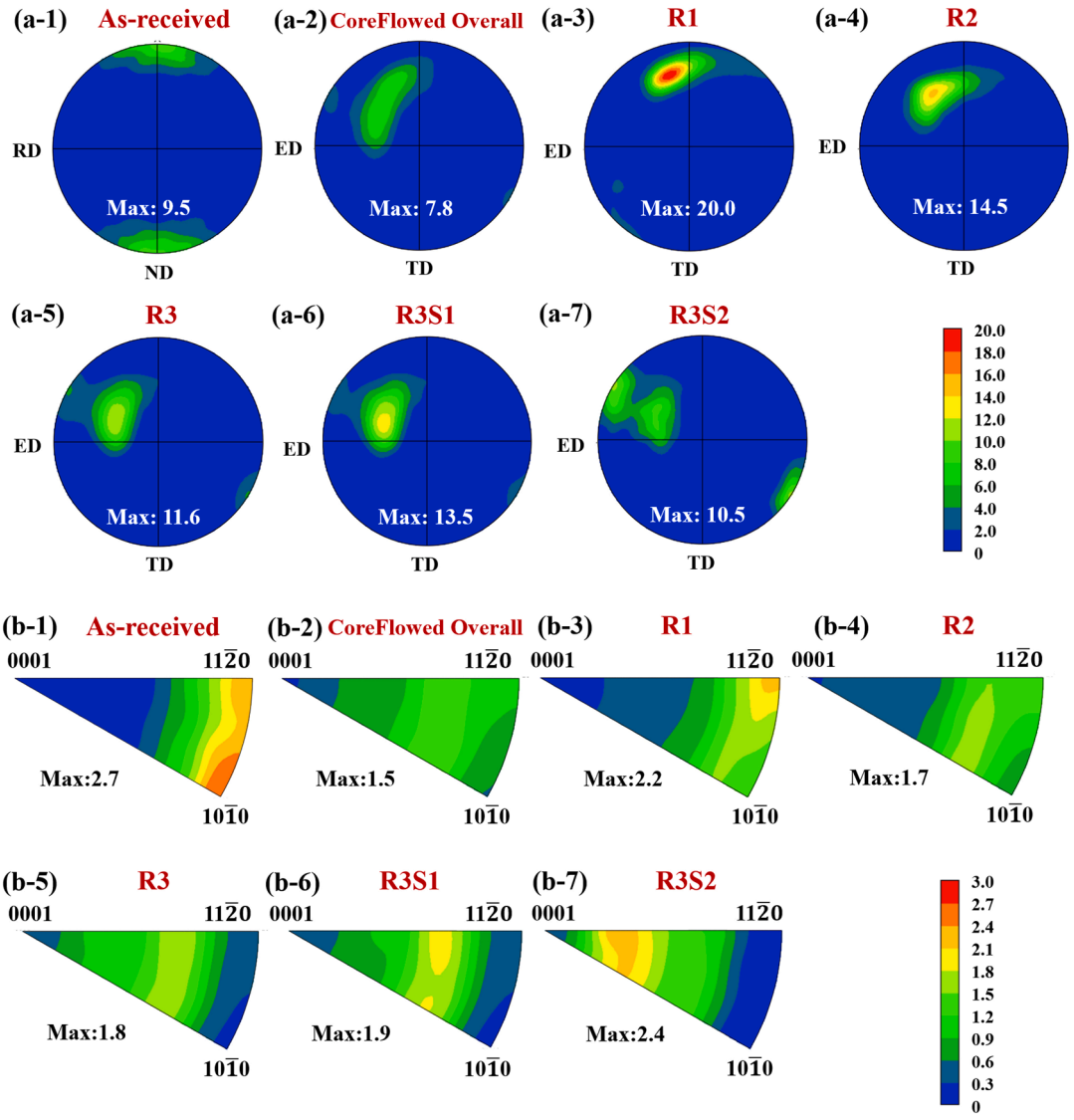

Fig. 2. (a-1)-(a-7) PFs and (b-1)-(b-7) IPFs of as-received and CoreFlowed AZ31B.

Based on these, the CoreFlowed wire was divided into three different regions R1–R3, and R3 can be subdivided into R3S1 region and R3S2 region due to their distinctive characteristics (Fig. 2). It is apparent that the basal pole orientations of these regions were different. From R1 to R3 (i.e. core to edge), the basal pole gradually rotated towards the ED. In R3, two basal pole peaks were observed corresponding to R3S1 and R3S2. More specifically, the shift of the basal pole from R1 to R3S1 was continuous, whilst the basal pole of R3S2 tended to shift toward a different direction. The IPFs also shows different texture components from R1 to R3. The IPF of R1 indicates that the <11-20> directions of grains mainly aligned along ED. When it comes to R2 and R3, the <0001> direction gradually rotates toward ED, becoming more off-basal. R3S1 and R3S2 also showed a difference, between which R3S2 tended to be more off-basal.

BSE images of as-received and CoreFlowed AZ31B are shown in Fig. 3. Second phase particles in the as-received sample were mainly elongated and linearly aligned along the RD, although a few equiaxed particles with a larger size were also noted. This is common for rolled AZ31B, during which second phase particles are elongated along the rolling direction and then broken and become discontinuous. While in the CoreFlowed sample, along both ED and TD, second phase particles tend to be round, and the distribution was also homogeneous. No obvious clustering was observed in CoreFlowed sample. XCT results further revealed the 3D distribution of second particles in the CoreFlowed (Fig. 3, Video S2). Second phase particles were homogeneously distributed, as shown in the BSE images, and internal voids were hardly observed. A cylindrical volume was also extracted to investigate the 3D information of second phase particles. The size and distribution of second phase particles were homogeneous throughout the CoreFlowed sample.

The tensile properties are shown in Table 1. Representative engineering and true stress-strain curves are also plotted in Fig. 4(a). The El was significantly improved by nearly 58% via CoreFlow^{TM}, without noticeable compromise in strength. The typical SEM images of fractured surfaces after tensile tests are shown in Fig. 4(b) and (c). The fractured surface of as-received sample exhibited well-defined step patterns and shallow dimples. Whilst in the CoreFlowed sample the fractured surface was dominated by much deeper dimples of different size, indicating increased ductility deformation modes.

The texture and microstructure differences are believed to be the result of the complex material flow during CoreFlow^{TM}. Considering the similarity between these two technologies, a hypothesis of the CoreFlow^{TM} process can be developed based on previous research on FSE [33–35]. During processing, the base material was firstly cut and extracted by the 8-thread probe (Fig. S1) when it was rotating and moving forward. These materials were transported with the rotation of

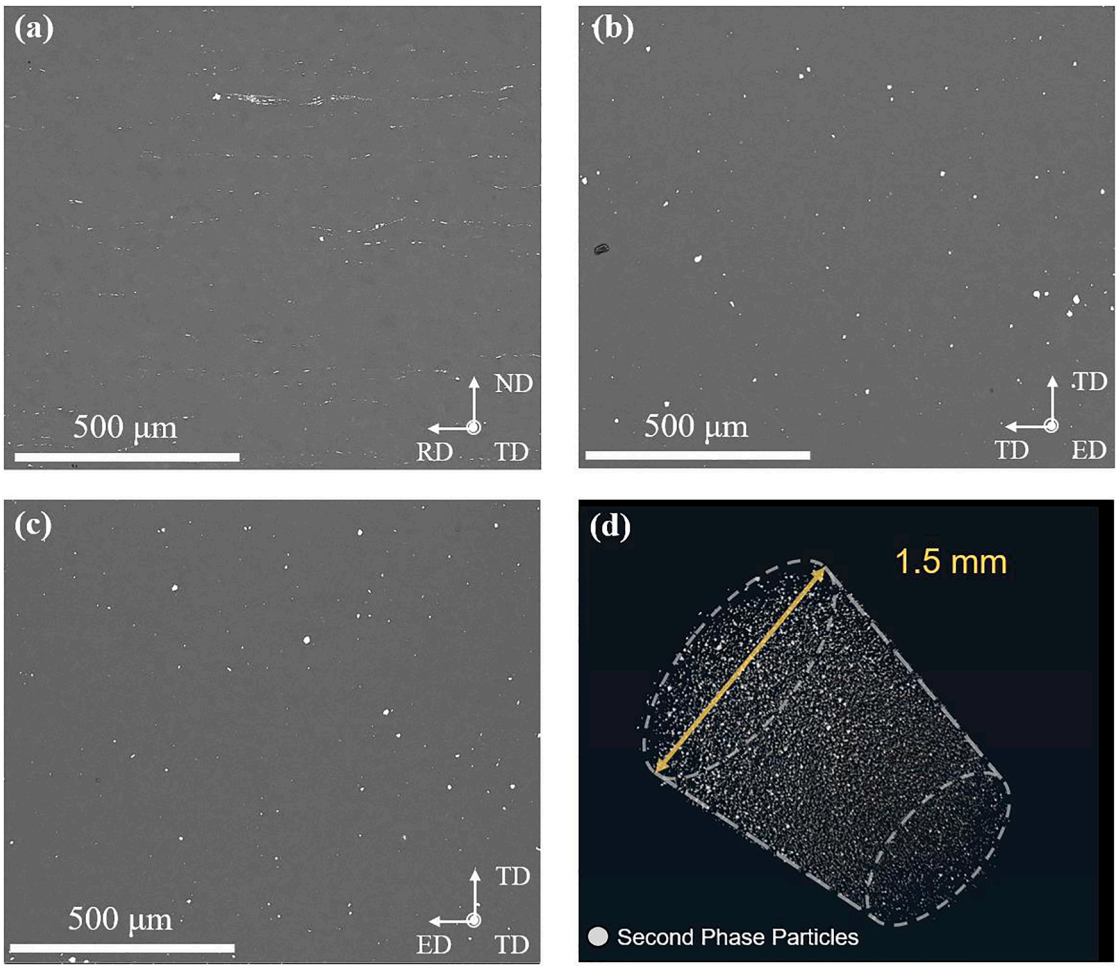

Fig. 3. BSE images of (a) as-received AZ31B along TD, (b) CoreFlowed AZ31B along ED, (c) CoreFlowed AZ31B along TD, (d) A 3D view of second phase particles in a cylindrical volume extracted from CoreFlowed AZ31B XCT result.

Table 1
Mechanical properties of as-received and CoreFlowed AZ31B.

Material	YS(MPa)	UTS (MPa)	El (%)
As-received AZ31B	137 ± 9	260 ± 1	14.1 ± 0.3
CoreFlowed AZ31B	134 ± 6	258 ± 5	22.3 ± 0.8

the tool and welded together in a helical mode in the region where threads end. Then the consolidated material was extruded through the channel and air cooled.

To validate this hypothesis, a simple calculation (Eq (1)) based on R3S2 (Fig. 2(b-1)) was carried out. Although no valid evidence can justify it, several findings support this hypothesis. If the aforementioned hypothesis is correct, then it follows that:

$$2D = ndtan\theta \quad (1)$$

where D is the diameter of the wire, n is the number of threads on the probe, d is the distance between each R3S2 region, and θ is the angle between R3S2 region and ED axis. In this work, D was 2 mm, d and $tan\theta$ was measured to be 0.31 mm and 1.65. The calculated value of n was about 7.82, which is very close to the actual number of threads 8. EBSD IPF maps also support the hypothesis. The texture of the as-received and CoreFlowed AZ31B samples were significantly different from center to edge, which is attributed to different conditions during CoreFlow^{TM}. Based on IPFs shown in Fig. 2(b-1)–(b-7), the as-received AZ31B developed a strong basal texture which is very typical in conventional Mg alloys such as AZ31B. While for CoreFlowed AZ31B, the strain path of R1 is similar to that of extrusion, represented by basal fibre texture components with <10-10> or <11-20> directions parallel to the extrusion direction [36]. However, there were also a range of non-specific directions in the basal plane. The basal fibre texture with <11-20>//ED is usually related to the recrystallised texture, which is consistent with the CoreFlowed AZ31B where dynamic recrystallisation (DRX) occurred.

For R2 and further to R3, the peak in the IPFs moves toward <0001>, indicating the texture further deviates from the "extrusion condition". This continuous shift from R1 to R3S1 is attributed to the enhanced effect of rotation at the edge. In contrast to R3S1, the basal pole of R3S2 tends to shift to a different direction. This is attributed to the seam welding between materials extracted from neighbouring threads. This explains why these needle-like regions have limited thickness, different orientations from neighbouring regions, and periodicity. In addition to the texture, the complex material flow also triggered grain refinement and microstructural modification. The grain refinement effect is attributed to the DRX during processing [37]. Considering the low stacking fault energy, possibly high total strain and high temperature during CoreFlow^{TM}, continuous dynamic recrystallisation (CDRX) should be the dominant mode [37]. Commonly observed internal grain misorientation and well-defined subgrain boundaries validate the prominent occurrence of CDRX (Fig. S5). Some grains had hardly deformed and incomplete CDRX grains over 20 μm remained in CoreFlowed AZ31B, forming a heterogeneous structure within the small DRXed grains. The friction stirring effect also generated a redistribution

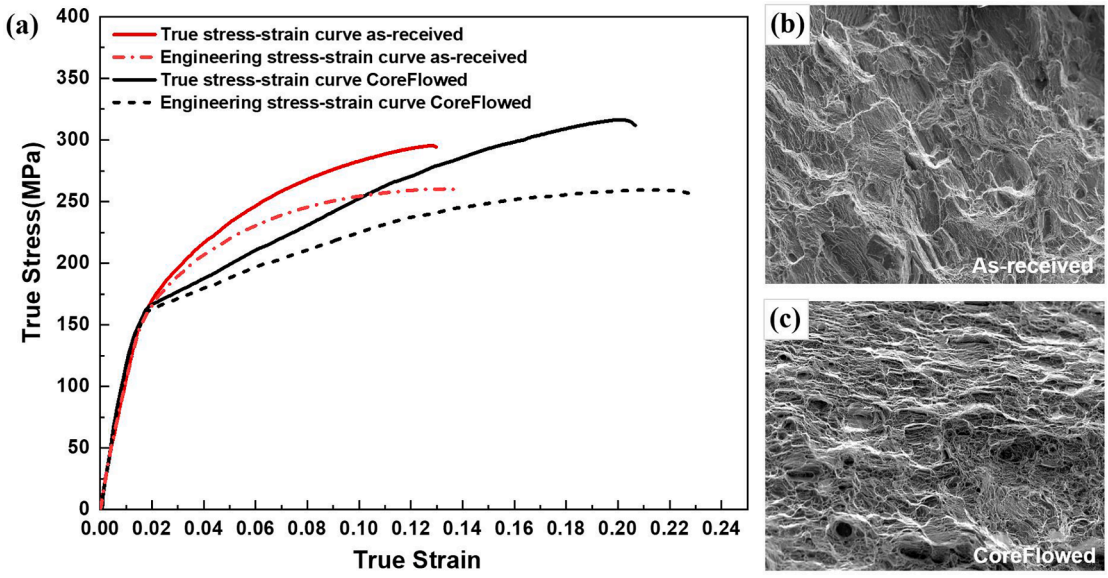

Fig. 4. (a) Engineering and true stress-strain curves of CoreFlowed and as-received AZ31B, (b) SE image of fractured surface of as-received AZ31B, (c) SE image of fractured surface of CoreFlowed AZ31B.

of second phase particles. The approximately linear size distribution of elongated second phase particles was transformed into a more homogenous distribution of rounder second phase particles throughout the whole wire.

It is unexpected that the yield strength was not improved by the grain refinement. According to Hall-Petch relationship (Eq (2)),

$$\sigma = \sigma_0 + kd^{-\frac{1}{2}} \tag{2}$$

the strength σ increases when the grain size d decreases. However, no strengthening was observed in the CoreFlowed AZ31B after grain refinement. Zhang et al. [17] developed a fine bimodal grain structure in a Mg-3Al-1Zn-0.4Mn alloy with an average grain size of 8.2 μm, which is slightly coarser than the 6.5 μm obtained here. The calculated yield strength from the Hall-Petch relationship was much higher than the experimentally observed value, as found here, Fig. 4a. As analyzed by Berbenni et al. [38], the average grain size is not a good predictor of yield strength where a heterogeneous grain size is present. Their analysis showed that an increase in the dispersion of grain size results in a decrease in yield strength. This was believed to be associated with the internal stress and elastic stored energy between grains. Yuan et al. [39] and Chen et al. [40] indicated that the grain orientation plays an important role in the yield behavior of Mg alloys. The soft orientation for basal slip activation tends to generate lower YS, which is the case in the CoreFlowed samples even CoreFlowed samples have refined grains compared to as-received samples.

Nevertheless, CoreFlowed samples showed a significant increase in the total elongation of ~58% compared to as-received AZ31B sheet, achieving a total elongation of ~22%. Such a good combination of strength and elongation (UTS 258 ± 5 MPa and EI 22.3 ± 0.8%) is not common. These properties are ascribed not only to the fine average grain size (6.5 μm) but also the grain size distribution. Zhang et al. [17] undertook a careful analysis of the strain developed within grains in a Mg-3Al-1Zn-0.4Mn alloy with a similar grain size distribution to that developed in the current work, which also showed high work hardening. They demonstrated that the high work hardening was associated with the grain size difference. A significant difference in microstrain was found between "large" and "small" grains, leading to a pile-up of geometrically necessary dislocations (GNDs) at the grain boundaries between the large and small grains, which they believed was responsible for the high work hardening rate. Moreover, a significant increase of non-basal dislocations was observed as strain increased, which they believed was responsible for ductility improvement.

The weakening of the texture by the CoreFlow™ process will have played a part in achieving high uniform elongation. The weakened texture offers a wider spread of grain orientations and this is believed to allow more grains with a soft crystal orientation to accommodate plastic deformation. Moreover, non-basal slips would have been easier to activate with the weakened texture compared to the as-received hot rolled AZ31 plate with strong basal texture [17]. Such non-basal slip is usually considered to play an important role in improving the ductility of Mg alloys. In addition to the factors discussed above, the greatly improved homogeneity of the second phase particles, in terms of distribution, size and shape, will have aided superior ductility.

In summary, an AZ31B Mg alloy wire was successfully produced using CoreFlow™ in a single step at room temperature for the first time. Compared with the as-received material, CoreFlowed AZ31B exhibited finer grains with heterogeneous grain size distribution due to DRX. A weakened texture with gradient evolution from center to edge and periodic needle-like regions with a distinctively different orientation from neighbouring regions around edge area was observed. These texture characteristics are assumed to be the result of friction stir, extrusion, and seam welding during the process. The UTS and El of the CoreFlowed sample reached 258 ± 5 MPa and 22.3 ± 0.8%, respectively. Such a good combination of strength and ductility for AZ31B Mg alloy is believed to be a result of grain refinement with a heterogeneous grain size distribution, texture weakening, and homogeneously distributed second phase particles.

Declaration of Competing Interest

The authors declare that they have no known competing financial interests or personal relationships that could have appeared to influence the work reported in this paper.

Acknowledgments

This work was supported by the UKRI MRC Future Leaders Fellowship, [MR/T019123/1]. We wish to acknowledge the Henry Royce Institute for Advanced Materials, funded through EPSRC grants [EP/R00661X/1, EP/S019367/1, EP/P02470X/1 and EP/P025285/1], for JSM-7900F FESEM/EBSD access at The University of Sheffield. Authors also acknowledge the XCT access supported by University of Sheffield

Tomography Center (STC) funding from EPSRC [EP/T006390/1], and support from the National Research Facility for Lab X-ray CT (NXCT) through EPSRC grant [EP/T02593X/1].

Supplementary materials

Supplementary material associated with this article can be found, in the online version, at doi:10.1016/j.scriptamat.2023.115301.

References

[1] Z. Zeng, N. Stanford, C.H.J. Davies, J.F. Nie, N. Birbilis, Magnesium extrusion alloys: a review of developments and prospects, Int. Mater. Rev. 64 (1) (2018) 27–62.
[2] F. Pan, M. Yang, X. Chen, A review on casting magnesium alloys: modification of commercial alloys and development of new alloys, J. Mater. Sci. Technol. 32 (12) (2016) 1211–1221.
[3] B.C. Suh, M.S. Shim, K.S. Shin, N.J. Kim, Current issues in magnesium sheet alloys: where do we go from here? Scr. Mater. 84-85 (2014) 1–6.
[4] S. Shamsudin, M.A. Lajis, Z.W. Zhong, Solid-state recycling of light metals: a review, Adv. Mech. Eng. 8 (8) (2016) 1–23.
[5] J. Zhao, B. Jiang, A. Tang, Y. Chai, B. Liu, H. Sheng, T. Yang, G. Huang, D. Zhang, F. Pan, Deformation behavior and texture evolution in an extruded Mg Li sheet with non-basal texture during tensile deformation, Mater. Charact. 159 (2020) 110041.
[6] L. Guo, J. Yuan, J. Pei, Y. Zhao, K. Zhang, J. Jiang, Study of the microstructure, bonding evolution and mechanical properties of continuously extruded magnesium AZ31 sheet, Mater. Sci. Eng. A 819 (2021) 141456.
[7] J.F. Nie, K.S. Shin, Z.R. Zeng, Microstructure, deformation, and property of wrought magnesium alloys, Metall. Mater. Trans. A 51 (12) (2020) 6045–6109.
[8] K.K. Alaneme, E.A. Okotete, Enhancing plastic deformability of Mg and its alloys—a review of traditional and nascent developments, J. Magnes. Alloy. 5 (4) (2017) 460–475.
[9] A. Imandoust, C.D. Barrett, T. Al-Samman, K.A. Inal, H. El Kadiri, A review on the effect of rare-earth elements on texture evolution during processing of magnesium alloys, J. Mater. Sci. 52 (1) (2016) 1–29.
[10] G. Zhang, Z. Zhang, X. Li, Z. Yan, X. Che, J. Yu, Y. Meng, Effects of repetitive upsetting-extrusion parameters on microstructure and texture evolution of Mg–Gd–Y–Zn–Zr alloy, J. Alloy. Compd. 790 (2019) 48–57.
[11] Z. Abbasi, R. Ebrahimi, J.M. Cabrera, Investigation on texture evolution and recrystallization aspects of novel Mg–Zn–Gd–Y–Nd Alloys, Met. Mater. Int. 27 (10) (2020) 3983–3992.
[12] D. Guan, X. Liu, J. Gao, L. Ma, B.P. Wynne, W.M. Rainforth, Exploring the mechanism of “Rare earth” texture evolution in a lean Mg–Zn–Ca alloy, Sci. Rep. 9 (1) (2019) 7152.
[13] Q. Wu, H. Yan, J. Chen, W. Xia, M. Song, B. Su, T. Ding, Dynamic precipitation, dynamic recrystallization, and texture evolution of Mg-5Zn alloy sheets with trace Ca and Sr additions, Microsc. Microanal. 26 (5) (2020) 886–894.
[14] J. Wu, L. Jin, J. Dong, F. Wang, S. Dong, The texture and its optimization in magnesium alloy, J. Mater. Sci. Technol. 42 (2020) 175–189.
[15] L.Y. Zhao, H. Yan, R.S. Chen, E.H. Han, Oriented nucleation causing unusual texture transition during static recrystallization annealing in cold-rolled Mg–Zn–Gd alloys, Scr. Mater. 188 (2020) 200–205.
[16] V. Segal, Review: modes and processes of severe plastic deformation (SPD), Materials 11 (7) (2018).
[17] Z. Zhang, J. Zhang, W. Wang, S. Liu, B. Sun, J. Xie, T. Xiao, Unveiling the deformation mechanism of highly deformable magnesium alloy with heterogeneous grains, Scr. Mater. 221 (2022) 114963.
[18] Z.R. Zeng, Y.M. Zhu, R.L. Liu, S.W. Xu, C.H.J. Davies, J.F. Nie, N. Birbilis, Achieving exceptionally high strength in Mg 3Al 1Zn-0.3Mn extrusions via suppressing intergranular deformation, Acta Mater. 160 (2018) 97–108.
[19] P. Mansoor, S.M. Dasharath, Microstructural and mechanical properties of magnesium alloy processed by severe plastic deformation (SPD) – a review, Mater. Today Proc. 20 (2020) 145–154.
[20] P. Minárik, J. Veselý, R. Král, J. Bohlen, J. Kubásek, M. Janeček, J. Stráská, Exceptional mechanical properties of ultra-fine grain Mg-4Y-3RE alloy processed by ECAP, Mater. Sci. Eng. A 708 (2017) 193–198.
[21] T. Krajňák, P. Minárik, J. Gubicza, K. Máthis, R. Kužel, M. Janeček, Influence of equal channel angular pressing routes on texture, microstructure and mechanical properties of extruded AX41 magnesium alloy, Mater. Charact. 123 (2017) 282–293.
[22] H. Utsunomiya, K.I. Izumi, T. Sakai, T. Mukai, Grain refinement of magnesium alloy sheets by ARB using high-speed rolling mill, J. Phys. Conf. Ser. 165 (2009), 012011.
[23] A.A. Nia, H. Omidvar, S.H. Nourbakhsh, Effects of an overlapping multi-pass friction stir process and rapid cooling on the mechanical properties and microstructure of AZ31 magnesium alloy, Mater. Des. 58 (2014) 298–304.
[24] C. Chang, X. Du, J. Huang, Producing nanograined microstructure in Mg–Al–Zn alloy by two-step friction stir processing, Scr. Mater. 59 (3) (2008) 356–359.
[25] K.P. Mehta, P. Vilaça, A review on friction stir-based channeling, Crit. Rev. Solid State Mater. Sci. 47 (1) (2021) 1–45.
[26] G.K. Padhy, C.S. Wu, S. Gao, Friction stir based welding and processing technologies - processes, parameters, microstructures and applications: a review, J. Mater. Sci. Technol. 34 (1) (2018) 1–38.
[27] C.I. Chang, X.H. Du, J.C. Huang, Achieving ultrafine grain size in Mg–Al–Zn alloy by friction stir processing, Scr. Mater. 57 (3) (2007) 209–212.
[28] Z. Zulkfli, N. Fatchurrohman, Advancement in friction stir processing on magnesium alloys, Conf. Ser. Mater. Sci. Eng. 1092 (2020), 012006.
[29] J. Peng, Z. Zhang, Z. Liu, Y. Li, P. Guo, W. Zhou, Y. Wu, The effect of texture and grain size on improving the mechanical properties of Mg-Al-Zn alloys by friction stir processing, Sci. Rep. 8 (1) (2018) 4196.
[30] W. Wang, P. Han, P. Peng, T. Zhang, Q. Liu, S.N. Yuan, L.Y. Huang, H.L. Yu, K. Qiao, K.S. Wang, Friction stir processing of magnesium alloys: a review, Acta Metall. Sin. Engl. Lett. 33 (1) (2019) 43–57.
[31] B. Darras, E. Kishta, Submerged friction stir processing of AZ31 magnesium alloy, Mater. Des. 47 (2013) 133–137.
[32] M. Sabbaghian, R. Mahmudi, Superplasticity of the fine-grained friction stir processed Mg–3Gd–1Zn sheets, Mater. Charact. 172 (2021) 110902.
[33] G. Buffa, D. Campanella, L. Fratini, F. Micari, AZ31 magnesium alloy recycling through friction stir extrusion process, Int. J. Mater. Form. 9 (5) (2015) 613–618.
[34] D. Baffari, G. Buffa, L. Fratini, Influence of process parameters on the product integrity in friction stir extrusion of magnesium alloys, Key Eng. Mater. 716 (2016) 39–48.
[35] D. Baffari, G. Buffa, L. Fratini, A numerical model for wire integrity prediction in friction stir extrusion of magnesium alloys, J. Mater. Process. Technol. 247 (2017) 1–10.
[36] M.G. Jiang, C. Xu, H. Yan, G.H. Fan, T. Nakata, C.S. Lao, R.S. Chen, S. Kamado, E. H. Han, B.H. Lu, Unveiling the formation of basal texture variations based on twinning and dynamic recrystallization in AZ31 magnesium alloy during extrusion, Acta Mater. 157 (2018) 53–71.
[37] A. Heidarzadeh, S. Mironov, R. Kaibyshev, G. Çam, A. Simar, A. Gerlich, F. Khodabakhshi, A. Mostafaei, D.P. Field, J.D. Robson, A. Deschamps, P. J. Withers, Friction stir welding/processing of metals and alloys: a comprehensive review on microstructural evolution, Prog. Mater. Sci. 117 (2021).
[38] S. Berbenni, V. Favier, M. Berveiller, Impact of the grain size distribution on the yield stress of heterogeneous materials, Int. J. Plast. 23 (1) (2007) 114–142.
[39] W. Yuan, S.K. Panigrahi, J.Q. Su, R.S. Mishra, Influence of grain size and texture on Hall–Petch relationship for a magnesium alloy, Scr. Mater. 65 (11) (2011) 994–997.
[40] W.Z. Chen, X. Wang, M.N. Kyalo, E.D. Wang, Z.Y. Liu, Yield strength behavior for rolled magnesium alloy sheets with texture variation, Mater. Sci. Eng. A 580 (2013) 77–82.